

# Elastic solution for liquid-bridging-induced microscale contact

H. Fan<sup>a)</sup> and Y. X. Gao

*Center for Mechanics of Micro-Systems, School of Mechanical and Production Engineering, Nanyang Technological University, Singapore 639798, Singapore*

(Received 23 March 2001; accepted for publication 31 August 2001)

Microscale contact between two solid surfaces induced by the liquid-bridging force is studied in the present article. Attention is focused on the interaction between the size of the contact area and the magnitude of the liquid-bridging force. The liquid-bridging force is related to the contact size and the other parameters, such as the filling angle, the contact angles, and the surface tension of the liquid, by solving the Laplace–Young equation. A singular integral equation for the coupled contact equilibrium problem is established and solved. Two approximate solutions for the same problem are also given and compared with the solution of the singular integral equation. Parametric study reveals the dependence of the semicontact width and the liquid-bridging force on the filling angle and the dimensionless group in the microscale contact. © 2001 American Institute of Physics.

[DOI: 10.1063/1.1415057]

## I. INTRODUCTION

When a small amount of liquid is placed around the area of contact between two solid surfaces, it spontaneously forms a liquid bridge and a meniscus surface between the slightly apart solid surfaces near the contact area. This is often called the liquid-bridging phenomenon, as illustrated in Fig. 1. The attractive force between the two solid surfaces, induced by the capillary force of the liquid and the surface tension of the meniscus surface, is called liquid-bridging force. The force is of little significance at high external load contacts. However, it becomes increasingly important as the load is reduced towards zero, and can make a significant contribution to the microscale contact equilibrium under the condition of zero external loading. The present article makes a detailed analysis for these equilibrium conditions.

In microsystems, the size of the devices is very small and the start-up force and driving torque to overcome friction and adhesion forces are necessarily small. Friction and adhesive retarding forces should assume a greater importance than that in the macroscopic world, and the factors that most significantly influence these retarding forces differ from those in the macroworld. Gravitational forces are negligible because of the small size and mass of micromechanical elements. However, the surface forces and interactions between the surfaces, such as electrostatic attraction and liquid-bridging force, are the most significantly influential factors on the microscale. For example, a typical head–disk spacing in magnetic recording hard disk drive systems is in the order of 100 nm. A protective carbon overcoat with an overlay of thin-film lubricant is used over the surface of the disk to separate the head slider from the disk and maintain low friction and wear.<sup>1</sup> However, the presence of the lubricant film and an adsorbed water droplet due to humidity can cause

meniscus rings around contacting asperities and liquid bridges between the head and the disk. The liquid-bridging force gives such a large contribution to the friction force that the head slider may get stuck over the disk surface.<sup>2,3</sup>

Liquid-bridging phenomena have been observed and studied by many researchers from various fields.<sup>3–8</sup> Earlier works (see, e.g., Ref. 5) showed that in a humid atmosphere remarkable adhesion was observed between solid surfaces. The adhesion depended on the humidity, and at saturation the adhesion was the same as that observed if a small drop of water was placed between the surfaces. This suggested that the observed adhesion should be due to the water adsorbed or deposited on the surfaces. Orr, Scriven, and Rivas<sup>8</sup> presented a detailed literature survey on the earlier works related to the meniscus properties and capillary force involved in the liquid bridging between two solid surfaces by means of solving the Laplace–Young equation (see Ref. 9). These works mainly discussed the aspects of liquid mechanics, including the volume of liquid, surface area, and mean curvature of the meniscus, and the liquid-bridging forces exerted on the solid surfaces. It was noted that the earlier research works did not discuss the effect of the solids deformation induced by liquid-bridging forces, namely, the solids were considered as rigid bodies. Recent works<sup>7,10,11</sup> have studied the liquid-mediated contact in microtribology systems and discussed the contribution to the real contact area by liquid-bridging forces in terms of the well-known Hertzian solution for the contact between a sphere and a plane and the Greenwood–Williamson model<sup>12</sup> for rough surface contact. The liquid-bridging force was added into the normal force as the external force to estimate the contribution of the liquid-bridging force to the real contact area as well as the fiction. Nevertheless, the coupling interaction between the contact area and the liquid-bridging force was not addressed.

It is suspected that the magnitude of the liquid-bridging force and the area of contact between two deformable solids could be significantly coupled under certain conditions.

<sup>a)</sup> Author to whom correspondence should be addressed; electronic mail: mhfan@ntu.edu.sg

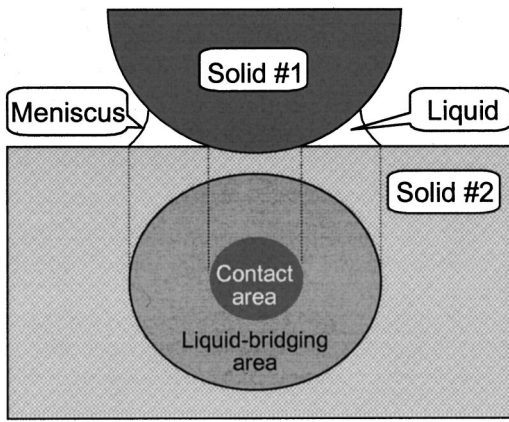


FIG. 1. Liquid-bridging-induced contact between an asperity and a half space.

Therefore, a coupled solution for a single asperity in contact with a plane, also interacting with liquid bridging, is essential for studying the contact between roughness surfaces and the contribution to friction in microtribology systems in a humid atmosphere. The aim of the present study is to obtain an exact mathematical solution for this coupled microscale contact problem.

**II. LIQUID-BRIDGING FORCE**

Let us consider a two-dimensional plane strain problem in which a rigid cylinder is in contact with the surface of an elastic half space without external load. A small liquid drop is introduced between the surfaces of the cylinder and the half space. The liquid wets with the two solid surfaces and forms the liquid bridging between the solid surfaces. Attractive force between the two solid surfaces induced by the liquid-bridging force produces a finite contact radius  $c$ , as shown in Fig. 2. Equilibrium is eventually established between the contact pressure and the liquid-bridging force. The equilibrium configuration of a solid/liquid/vapor system, including the meniscus and the triple-point line at the junction of the liquid, the solid, and the vapor, is described by the so-called Laplace–Young equation,

$$\Delta p = \kappa \gamma_{LV}, \quad \text{on the meniscus,} \tag{1}$$

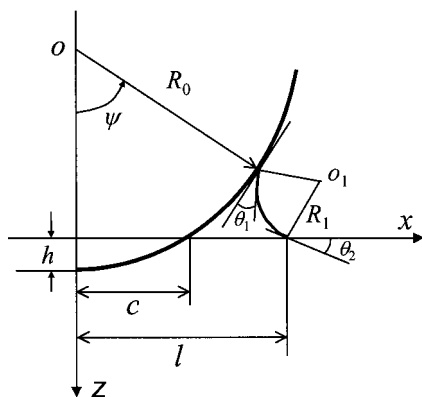


FIG. 2. Parameters of describing equilibrium configuration of the contact induced by the liquid bridging.

$$\gamma_{SV} = \gamma_{LS} + \gamma_{LV} \cos \theta, \quad \text{on the triple-point line.} \tag{2}$$

In Eq. (1),  $\Delta p$  is the difference in hydrostatic pressure across the meniscus interface and  $\kappa$  is the local mean curvature of the meniscus. In Eq. (2),  $\theta$  stands for the equilibrium contact angle at a triple-point line, and  $\gamma_{SV}$ ,  $\gamma_{LS}$ , and  $\gamma_{LV}$  denote the surface tensions between the liquid, vapor, and solid, respectively. In Fig. 2,  $\theta_1$  and  $\theta_2$  denote the equilibrium contact angles at the two triple-point lines. One is on the cylinder surface and another on the half-space surface. They are system constants. Other parameters shown in Fig. 2 are geometric parameters.  $R_0$  is the radius of the cylinder,  $\psi$  is the filling angle that characterizes the volume of the small liquid drop, and  $l$  is the size of the liquid-bridging area on the plane.

Since the characteristic length considered in the present analysis is so small, the effect of gravity can be negligible and the mean curvature is assumed to be nearly uniform. In other words, the meniscus profile can be modeled by an arc of the circle, as shown in Fig. 2. Following Orr’s scheme,<sup>8</sup> we obtain the mean curvature of the meniscus as

$$\kappa = \frac{\cos(\theta_1 + \psi) + \cos \theta_2}{R_0(1 - \cos \psi) - h}, \tag{3}$$

where  $h$  denotes the height of the part of the rigid cylinder in contact with the half space in the equilibrium state, as shown in Fig. 2.

Substituting Eq. (1) into Eq. (3), we obtain

$$\Delta p = \gamma_{LV} \left[ \frac{\cos(\theta_1 + \psi) + \cos \theta_2}{R_0(1 - \cos \psi) - h} \right]. \tag{4}$$

With Eq. (3), the dependence of the liquid-bridging area on filling angle  $\psi$  and contact angle  $\theta_1$  as well as  $\theta_2$  is given by

$$l = R_0 \sin \psi + R_1 [\sin(\theta_1 + \psi) - \sin \theta_2] \tag{5}$$

with

$$R_1 = \frac{R_0(1 - \cos \psi) - h}{\cos(\theta_1 + \psi) + \cos \theta_2}. \tag{6}$$

As another important issue in the present contact problem, the liquid-bridging force is formulated based on the above-given relations. The total force exerted through the liquid bridge between the cylinder and the half space consists of two parts, namely, a surface tension force that resides in the meniscus, and a capillary pressure force due to the hydrostatic pressure difference across the liquid/vapor interface. If attractive force between the cylinder and the half space is taken as positive, the axial component of the surface tension force per unit length is

$$F_s = 2 \gamma_{LV} \sin \theta_2, \tag{7}$$

and the capillary pressure force per unit length is

$$F_p = 2 \Delta p (l - c). \tag{8}$$

Hence, the total liquid-bridging force per unit length in the  $z$  direction is given by

$$F_{lb} = 2 [\gamma_{LV} \sin \theta_2 + \Delta p (l - c)]. \tag{9}$$

With the help of Eqs. (4)–(6), Eq. (9) shows that the liquid-bridging force not only depends on the geometrical and

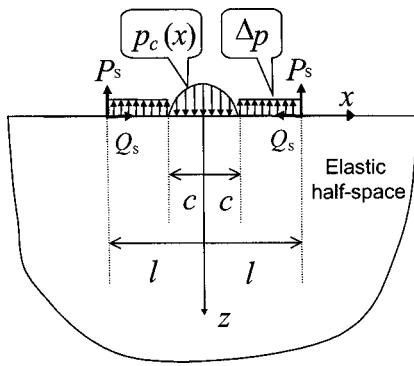


FIG. 3. Traction distribution on the surface of the elastic half space under contact.

physical parameters (the filling angle, the contact angles, and the surface tension); but also the deformation parameters (semicontact width  $c$  and contact height  $h$ ). In other words, we have to obtain the contact size induced by the liquid-bridging force in order to determine the magnitude of the liquid-bridging force. On the other hand, we have to obtain the liquid-bridging force to determine the contact size and the contact stress distribution. Obviously, the liquid-bridging force and the size of the contact area induced by the liquid bridge are coupled together.

### III. SOLUTION FOR LIQUID-BRIDGING-INDUCED CONTACT

Owing to the coupling feature discussed above, we have to solve the contact problem due to liquid bridging in order to determine the magnitude of the liquid-bridging force and the contact size as well as the contact stress distribution simultaneously. Let us consider a boundary value problem as follows. For the loaded elastic half space shown in the cross section in Fig. 3, the traction on the surface of the half space by the rigid cylinder is replaced by the contact pressure,  $p_c(x), x \in [-c, c]$ , in which both semicontact width  $c$  and contact pressure function  $p_c(x)$  are unknown. Besides the contact pressure, there are two kinds of liquid-bridging-induced forces. One is the uniform traction due to the capillary pressure in the liquid-bridging area, whose magnitude  $\Delta p$  is the pressure difference across the liquid/vapor interface given by Eq. (4). Another is the surface tension force on the triple-point line on the surface of the half space, expressed as

$$P_s = \gamma_{LV} \sin \theta_2, \quad Q_s = \gamma_{LV} \cos \theta_2, \quad (10)$$

where  $P_s$  and  $Q_s$  are the normal and tangential components of the surface tension force, respectively. Uniform traction  $\Delta p$  acts on the surface over regions  $x \in [-l, -c]$  and  $x \in [c, l]$ , and concentrated components  $P_s$  and  $Q_s$  act on points  $x = \pm l$ . The remainder of the surface is free of traction. It is required to solve the stress field and the displacement field in the elastic half space under the above-mentioned boundary condition.

### A. Singular integral equation

Based on the linear-elastic contact mechanics (see Ref. 13), normal displacement  $\bar{u}_z(x)$  and its gradient  $\bar{u}'_z(x)$  throughout the surface ( $z=0$ ), due to all the traction on the surface, are given by

$$\begin{aligned} \bar{u}_z(x) = & -\frac{2(1-\nu^2)}{\pi E} \int_{-l}^l p(s) \ln|x-s| ds \\ & -\frac{2P_s(1-\nu^2)}{\pi E} [\ln|x-l| + \ln|x+l|] \\ & +\frac{Q_s(1-2\nu)(1+\nu)}{E} [H(x+l) - H(x-l)] \\ & + \text{Const.}, \end{aligned} \quad (11)$$

and

$$\begin{aligned} \bar{u}'_z(x) = & -\frac{2(1-\nu^2)}{\pi E} \int_{-l}^l p(s) \frac{ds}{x-s} -\frac{2P_s(1-\nu^2)}{\pi E} \left[ \frac{1}{x-l} \right. \\ & \left. +\frac{1}{x+l} \right] +\frac{Q_s(1-2\nu)(1+\nu)}{E} [\delta(x+l) - \delta(x-l)], \end{aligned} \quad (12)$$

with

$$p(x) = \begin{cases} \Delta p, & x \in [-l, -c] \cup [c, l] \\ p_c(x), & x \in [-c, c]. \end{cases} \quad (13)$$

In Eqs. (11) and (12),  $H(x)$  and  $\delta(x)$  stand for the Heaviside function and its derivative, the delta function, respectively. Also,  $E$  and  $\nu$  are the Young's modulus and the Poisson's ratio of the elastic half space.

It is noticed that normal displacement  $\bar{u}_z(x)$  and its gradient  $\bar{u}'_z(x)$  for the points within contact area  $x \in [-c, c]$  can be determined by the shape of the rigid cylinder,

$$\bar{u}_z(x) = d - \frac{x^2}{2R_0}, \quad x \in [-c, c], \quad (14)$$

$$\bar{u}'_z(x) = -\frac{x}{R_0}, \quad x \in [-c, c], \quad (15)$$

where  $d$  stands for the approach of distant points (see Ref. 13).

A combination of Eqs. (12) and (15) leads to

$$\int_{-c}^c \frac{p_c(s)}{x-s} ds = g(x), \quad x \in [-c, c], \quad (16)$$

with

$$g(x) = \frac{\pi E^*}{2R_0} x - \Delta p \ln \left( \frac{(x+l)(x-c)}{(x-l)(x+c)} \right) + P_s \left( \frac{1}{x-l} + \frac{1}{x+l} \right), \quad (17)$$

and

$$\frac{1}{E^*} = \frac{1-\nu^2}{E}. \quad (18)$$

It should be noted that the integral in Eq. (16) is defined by its principal value because it has a singularity at  $x=s$ . Equa-

tion (16) is known as a Cauchy-type singular integral equation of the first kind with the unknown function  $p_c(x)$ . For the sake of convenience, we introduce the dimensionless variable

$$\xi = \frac{x}{c}, \tag{19}$$

and define two new functions as

$$\begin{aligned} \bar{p}_c(\xi) &= p_c(c\xi), \\ \bar{g}(\xi) &= g(c\xi) = \frac{\pi c E^*}{2R_0} \xi - \Delta p \ln \left[ \frac{(\xi+t)(\xi-1)}{(\xi-t)(\xi+1)} \right] \\ &\quad + \frac{P_S}{c} \left( \frac{1}{\xi-t} + \frac{1}{\xi+t} \right), \end{aligned} \tag{20}$$

with  $t=l/c$ . Then, Eq. (16) can be rewritten in the dimensionless form

$$\int_{-1}^1 \frac{\bar{p}_c(\eta)}{\xi-\eta} d\eta = \bar{g}(\xi), \quad \xi \in [-1, 1]. \tag{21}$$

It is obvious that the solution for Eq. (21) gives the contact pressure distribution.

### B. Chebyscheff series solution

According to Erdogan's scheme<sup>14</sup> for solving the singular integral equations, Eq. (21) can be solved by means of the well-known Chebyscheff polynomials. Because of its usefulness, the relation between the Chebyscheff polynomials of the first kind  $T_n(x)$  and the second kind  $U_n(x)$  are transcribed as

$$\int_{-1}^1 \frac{(1-y^2)^{1/2} U_{n-1}(y)}{x-y} dy = \pi T_n(x), \quad n=0, 1, 2, \dots \tag{22}$$

A comparison between Eqs. (21) and (22) suggests that the solution for Eq. (21) could be obtained by expanding the function  $\bar{g}(\xi)$  into the Chebyscheff series of the first kind. We expand the function  $\bar{g}(\xi)$  as

$$\bar{g}(\xi) = \sum_{n=0}^m A_n T_n(\xi) + O(\xi^{m+1}), \tag{23}$$

with  $A_n (n=0, 1, \dots, m)$  as the coefficients of the Chebyscheff series. Consequently, Eq. (22) reveals that the solution for Eq. (21) can be expressed in terms of the Chebyscheff polynomials of the second kind. With the help of Eq. (23), we have

$$\bar{p}_c(\xi) = \frac{1}{\pi} (1-\xi^2)^{1/2} \sum_{n=0}^m A_n U_{n-1}(\xi). \tag{24}$$

By using the first definition in Eq. (20), we finally obtain the contact pressure distribution

$$p_c(x) = \frac{1}{\pi} \left[ 1 - \left( \frac{x}{c} \right)^2 \right]^{1/2} \sum_{n=0}^m A_n U_{n-1}(x/c). \tag{25}$$

If one takes  $m$  sufficiently large, the series-form solution (25) should be as close as possible to the exact solution. In prac-

tice, however, the first few terms could provide a satisfactory result. In the following solution, we take  $m=5$ . In this case, the coefficients  $A_n$  in Eq. (23) can be determined by means of expanding the function  $\bar{g}(\xi)$  expressed by Eq. (20) into the Chebyscheff series:

$$\begin{aligned} A_1 &= \frac{\pi E^* c}{2R_0} - \Delta p \left[ \frac{2}{t} + \frac{1}{2t^3} + \frac{1}{4t^5} - \frac{11}{4} \right] \\ &\quad - \frac{P_S}{c} \left[ \frac{2}{t^2} + \frac{3}{2t^4} + \frac{5}{4t^6} \right], \\ A_3 &= -\Delta p \left[ \frac{1}{6t^3} + \frac{1}{8t^5} - \frac{7}{24} \right] - \frac{P_S}{c} \left[ \frac{1}{2t^4} + \frac{5}{8t^6} \right], \\ A_5 &= -\Delta p \frac{1}{40} \left[ \frac{1}{t^5} - 1 \right] - \frac{P_S}{c} \frac{1}{8t^6}, \\ A_0 &= A_2 = A_4 = 0. \end{aligned} \tag{26}$$

Therefore, function  $p_c(x)$  in the case of  $m=5$  is

$$\begin{aligned} p_c(x) &= \frac{1}{\pi} \left[ 1 - \left( \frac{x}{c} \right)^2 \right]^{1/2} [A_1 U_0(x/c) + A_3 U_2(x/c) \\ &\quad + A_5 U_4(x/c)]. \end{aligned} \tag{27}$$

The three Chebyscheff polynomials in Eq. (27) can be written as

$$U_0(\xi) = 1, \quad U_2(\xi) = 4\xi^2 - 1, \quad U_4(\xi) = 16\xi^4 - 12\xi^2 + 1. \tag{28}$$

A combination of Eqs. (27) and (28) leads to

$$\begin{aligned} p_c(x) &= \frac{1}{\pi} \left[ 1 - \left( \frac{x}{c} \right)^2 \right]^{1/2} \left[ 16A_5 \left( \frac{x}{c} \right)^4 + (4A_3 - 12A_5) \left( \frac{x}{c} \right)^2 \right. \\ &\quad \left. + A_1 - A_3 + A_5 \right]. \end{aligned} \tag{29}$$

Equation (29) with Eq. (26) provides the distribution of the contact pressure on the contact area.

Equation (25) or Eq. (29) cannot be uniquely defined before semicontact width  $c$  is determined. By considering the balance of the total normal load acting on the surface of the half space, we have

$$2P_S + 2\Delta p(l-c) = \int_{-c}^c p_c(x) dx. \tag{30}$$

Substituting solution (25) for  $p_c(x)$  into equilibrium Eq. (30), we obtain

$$2P_S + 2\Delta p(l-c) = \frac{c}{\pi} \sum_{n=0}^m A_n B_{n-1}, \tag{31}$$

with

$$B_{n-1} = \int_{-1}^1 (1-\xi^2)^{1/2} U_{n-1}(\xi) d\xi. \tag{32}$$

It is clear that Eq. (31) is a nonlinear algebra equation for  $c$  because of the coupled features among  $P_S$ ,  $\Delta p$ ,  $c$ , and  $h$ . From Eq. (14), it is not difficult to obtain the relationship between  $c$  and  $h$ ,

$$h = \bar{u}_z(0) - \bar{u}_z(c) = \frac{c^2}{2R_0}. \tag{33}$$

As a result, semicontact width  $c$  can be determined by solving algebra Eq. (31) with the help of Eqs. (5), (10), and (33). With the determined  $c$ , Eq. (25) gives a definite distribution of the contact pressure.

Since the liquid-bridging force and semicontact width are of our most interest, our parametric study explored the following dimensionless dependence implicitly given by the Chebyscheff series solution:

$$\frac{F_{lb}}{\gamma_{LV}} = f_{lb}(\chi, \psi, \theta_1, \theta_2), \tag{34}$$

$$\frac{c}{R_0} = f_c(\chi, \psi, \theta_1, \theta_2).$$

In Eq. (34), we introduced a dimensionless group  $\chi$  as

$$\chi = \frac{E^* R_0}{\gamma_{LV}}, \tag{35}$$

and  $f_{lb}$  and  $f_c$  denote the dimensionless functions.

We performed parametric studies for a specific example in which a water drop is assumed to be the liquid. Contact angles  $\theta_1$  and  $\theta_2$  are taken as  $60^\circ$  for demonstration purposes. Figures 4(a) and 4(b) show the dependence of the normalized liquid-bridging force on dimensionless group  $\chi$  and filling angle  $\psi$ , respectively, while Figs. 5(a) and 5(b) show the normalized semicontact width on them. The normalized liquid-bridging force increases rapidly as filling angle  $\psi$  decreases [see Fig. 4(b)]. The normalized semicontact width increases rapidly as the dimensionless group  $\chi$  decreases [see Fig. 5(a)]. Figure 5(b) shows that there exist maximum values of the normalized semicontact width as the filling angle decreases.

### C. Two approximated solutions

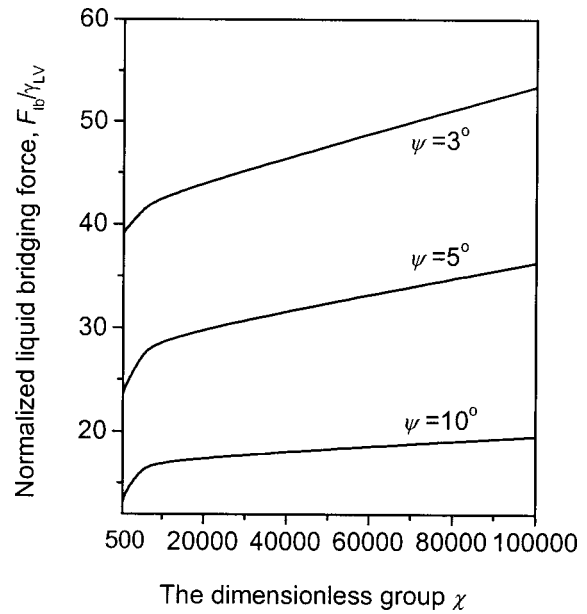
It can be seen that the Chebyscheff series solution is too complicated to be extended to the analysis of multiple asperity microscale contacts. Therefore, certain approximated solutions are needed for multiasperity contact modeling. In this section, we discuss two approximated solutions.

If the above-mentioned contact problem (refer to Fig. 3) is simplified as a Hertzian contact, namely, the composition of the liquid-bridging force is taken as an external force acting on the rigid cylinder, the semicontact width is given readily by the well-known Hertzian solution (see Ref. 13), i.e.,

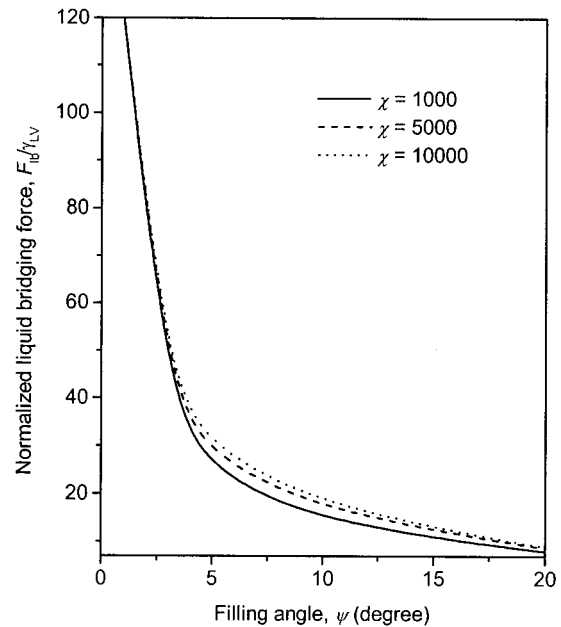
$$\frac{c}{R_0} = \left[ \frac{4}{\pi \chi} \frac{F_{lb}}{\gamma_{LV}} \right]^{1/2}. \tag{36}$$

The solution for Eqs. (9) and (36) gives us the semicontact width and liquid-bridging force. We, hereafter, refer to this solution as the *Hertzian approximation*. It is noted that semicontact width  $c$  and liquid-bridging force  $F_{lb}$  are still coupled together in this approximation.

If we ignore the contact-induced deformation when estimating the magnitude of the liquid-bridging force (see Refs.



(a)



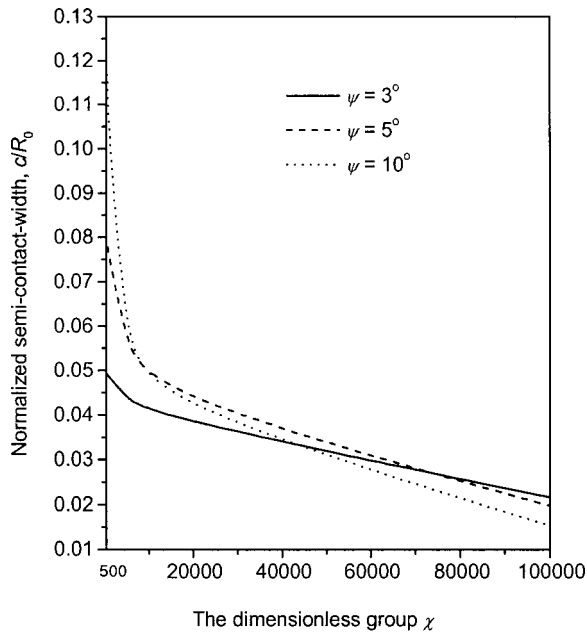
(b)

FIG. 4. Dependence of the normalized liquid-bridging force on (a) the dimensionless group  $\chi$  and (b) the filling angle  $\psi$ .

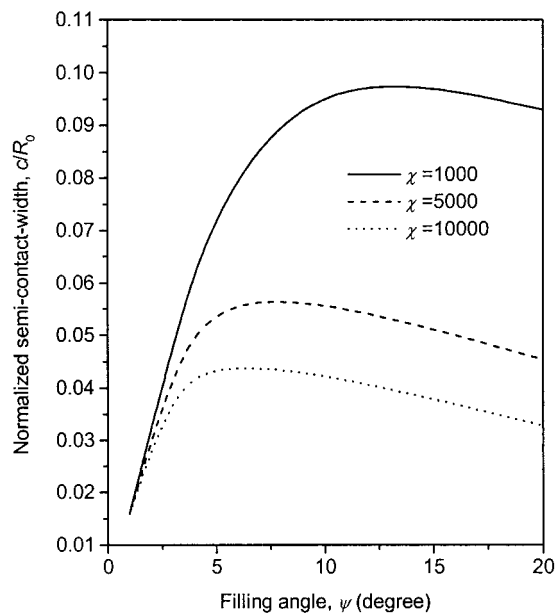
7 and 10), the above-mentioned contact problem can be decoupled. The liquid-bridging force no longer depends on the semicontact width and can be obtained readily by setting  $c = 0$  and  $h = 0$  in Eqs. (6) and (9),

$$\frac{F_{lb}}{\gamma_{LV}} = 2 \left[ \sin \theta_2 + \frac{l}{R_0} \frac{\cos(\theta_1 + \psi) + \cos \theta_2}{1 - \cos \psi} \right]. \tag{37}$$

Substitution of Eq. (37) into Eq. (36) gives the semicontact width directly. We, hereafter, refer to this solution as the *uncoupled approximation*.



(a)



(b)

FIG. 5. Dependence of the normalized semicontact width on (a) the dimensionless group  $\chi$  and (b) the filling angle  $\psi$ .

Tables I and II make the comparison among the solutions by use of the Chebyscheff series solution, and the Hertzian and uncoupled approximations, respectively. Table I [(a) and (b)] presents the normalized liquid-bridging force for various values of filling angle  $\psi$  with the specific dimensionless group (a)  $\chi = 10^3$  and (b)  $\chi = 10^5$ . Table II [(a) and (b)] presents the normalized semicontact width for various values of filling angle  $\psi$  with the specific dimensionless group (a)  $\chi = 10^3$  and (b)  $\chi = 10^5$ .

From Tables I and II, it is clear that for the cases of large  $\chi$  and large filling angle  $\psi$ , the three solutions are very close. In other words, the uncoupled approximation is able to ob-

tain satisfactory results for these cases. However, for small  $\chi$  and  $\psi$  the differences among the three solutions are considerably large. It implies that the coupling effect between the liquid-bridging force and the semicontact width is significant. Both the Chebyscheff series solution and Hertzian approximation have considered the coupling effect, and can be applied to deal with the microscale contact problems. Needless to say, the Chebyscheff series solution can give more exact results. It is seen that the uncoupled approximation overestimates the values of the liquid-bridging force and the contact area for very small  $\chi$  and  $\psi$ .

(a) Filling angle (degree)	5	10	20
Chebyscheff series solution	24.263	13.977	7.963
Hertzian approximation	17.451	12.862	7.864
Uncoupled approximation	44.075	21.128	9.611
(b) Filling angle (degree)	5	10	20
Chebyscheff series solution	36.274	19.565	9.376
Hertzian approximation	35.759	19.525	9.374
Uncoupled approximation	44.075	21.128	9.611

tain satisfactory results for these cases. However, for small  $\chi$  and  $\psi$  the differences among the three solutions are considerably large. It implies that the coupling effect between the liquid-bridging force and the semicontact width is significant. Both the Chebyscheff series solution and Hertzian approximation have considered the coupling effect, and can be applied to deal with the microscale contact problems. Needless to say, the Chebyscheff series solution can give more exact results. It is seen that the uncoupled approximation overestimates the values of the liquid-bridging force and the contact area for very small  $\chi$  and  $\psi$ .

#### IV. SUMMARY AND DISCUSSION

The present analytical solution provides a better understanding of liquid-bridging phenomena and the microscale contact induced by the liquid-bridging force. It is important for the further analysis of multiasperity contact between rough surfaces in a humid atmosphere in microtribology systems, where the components are very small in size and are operated under small driving forces. The equilibrium states of the liquid wetting between the slightly apart solid surfaces is governed by the Laplace–Young equation, while the solid contact induced by liquid bridging is governed by elastic contact mechanics. The most interesting phenomenon revealed by the numerical study is the coupling effect between the liquid-bridging force and the contact size. On the microscale, the coupling effect is considerable high and the contact

TABLE II. Comparison of the three solutions for the normalized semicontact width for various values of filling angles with the specific dimensionless group (a)  $\chi = 10^3$  and (b)  $\chi = 10^5$ .

(a) Filling angle (degree)	5	10	20
Chebyscheff series solution	0.0759	0.102	0.093
Hertzian approximation	0.149	0.128	0.100
Uncoupled approximation	0.237	0.164	0.111
(b) Filling angle (degree)	5	10	20
Chebyscheff series solution	0.0197	0.0153	0.0108
Hertzian approximation	0.0213	0.0158	0.0109
Uncoupled approximation	0.0237	0.0164	0.0111

problem has to be solved mathematically by an exact method, such as the Chebyscheff series solution. Our solutions reveal the dependence of the semicontact width and the liquid-bridging force on the filling angle and the dimensionless group.

It is worthwhile to mention that the present study addresses an elastic mechanics solution for a microscopic contact induced by a very small droplet of liquid, where the characteristic size, such as radius  $R_0$  of the rigid cylinder or liquid size  $R_0\psi$ , is very small. Therefore, one should be cautious when the characteristic size is so small that it exceeds the lowest bound of the linear dimension of a representative volume element for which the continuum hypothesis is applicable. In other words, elastic mechanics cannot provide solutions for problems beyond the continuum hypothesis. Statistical mechanics based considerations are required to deal with these problems.

- <sup>1</sup>F. E. Talke, *Wear* **190**, 232 (1995).
- <sup>2</sup>B. Bhushan, *Tribology and Mechanics of Magnetic Storage Devices* (Springer, New York, 1990).
- <sup>3</sup>C. Y. Poon and B. Bhushan, *Wear* **202**, 68 (1996).
- <sup>4</sup>J. S. McFarlane and D. Tabor, *Proc. R. Soc. London, Ser. A* **202**, 224 (1950).
- <sup>5</sup>F. P. Bowden and D. Tabor, D. Tabor, *Friction and Lubrication of Solids, Part I* (Oxford University Press, London, 1954).
- <sup>6</sup>F. P. Bowden and D. Tabor, *Friction and Lubrication of Solids, Part II* (Oxford University Press, London, 1964).
- <sup>7</sup>B. Bhushan, *Principles and Applications of Tribology* (Wiley, New York, 1999).
- <sup>8</sup>F. M. Orr, L. E. Scriven, and A. P. Rivas, *J. Fluid Mech.* **67**, 723 (1975).
- <sup>9</sup>R. Finn, *Equilibrium Capillary Surface* (Springer, New York, 1986).
- <sup>10</sup>C. Gao, X. Tian, and B. Bhushan, *Tribol. Trans.* **38**, 201 (1995).
- <sup>11</sup>X. Tian and B. Bhushan, *J. Phys. D* **29**, 163 (1996).
- <sup>12</sup>J. A. Greenwood and J. B. P. Williamson, *Proc. R. Soc. London, Ser. A* **295**, 300 (1966).
- <sup>13</sup>K. L. Johnson, *Contact Mechanics* (Cambridge University Press, Cambridge, 1985).
- <sup>14</sup>F. Erdogan, in *Mechanics Today*, edited by S. Nemat-Nasser (Pergamon, New York, 1978), Vol. 4, p. 1.